Optical vortex filtering for the detection of electromagnetically induced transparency

Nathaniel B. Phillips, Gleb V. Romanov, William F. Ames, and Irina Novikova*

Department of Physics, The College of William and Mary, Williamsburg, Virginia 23187, USA
**Corresponding author: inovikova@physics.wm.edu*

Received June 28, 2011; accepted July 6, 2011;
posted July 18, 2011 (Doc. ID 149838); published August 10, 2011

We report on the realization of an optical filter based on an optical vortex mask designed to exclusively detect a weak coherent laser field in the presence of a much stronger, nearly spatially overlapping field. We demonstrate the performance of such an optical vortex filter to eliminate the strong control field and detect only a weak optical field's transmission under the conditions of electromagnetically induced transparency. The attractive feature of such a filter is its insensitivity to optical field frequencies and polarizations, which makes it applicable for a wide range of coherent processes.

OCIS codes: 070.6110, 270.1670, 120.2440.

The problem of detecting a weak optical signal in the presence of other strong laser fields is inherent to many optical experiments. In particular, this problem arises in experiments involving electromagnetically induced transparency (EIT) [1,2], in which optical properties of a weak probe field can be coherently controlled by means of a strong classical control field. The most common EIT configuration is a three-level Λ system, shown in Fig. 1(a), in which the control and probe fields connect two long-lived hyperfine or Zeeman sublevels of the electronic ground state with a common excited level. In this case, the presence of the control field leads to a strong coupling between the probe field and a collective atomic spin excitation that results in strong suppression of resonant absorption, and opens a narrow window of transparency, $\Gamma_{\mathrm{EIT}} = |\Omega_C|^2/(\sqrt{d}\gamma)$, where Ω_C is the Rabi frequency associated with the control field and γ is the optical polarization decay rate. Here, we define the optical depth, $2d$, such that the probe intensity without EIT is attenuated by e^{-2d}. The accompanying steep normal dispersion allows for dramatic group velocity reduction $v_g \propto |\Omega_C|^2 L/(d\gamma) \ll c$ (slow light), where L is the length of the medium, and the reversible mapping of a probe pulse onto a long-lived atomic coherence (stored light) [2–4]. These phenomena present promising avenues toward technologies such as miniature atomic clocks and magnetometers [5,6], all-optical delay lines [4], single photon sources [7–9], and efficient quantum memories [10,11].

The exclusive detection of a weak probe field, especially at the few-photon level, in the presence of a strong control field, as in EIT experiments, becomes a challenging experimental task. Since the two optical fields have similar frequencies (differing by a few gigahertz for a Λ system based of different hyperfine ground state sublevels to a submegahertz difference for Zeeman sublevels of the same hyperfine manifold), traditional dichroic or interference filters are not effective, and thus only narrowband transmission elements (such as high-finesse Fabry–Perot etalons) [8,12,13] or high-quality polarizers (for orthogonally polarized control and probe fields) must be placed before a probe detector to suppress the control field. These filtering methods are often very sensitive to frequencies and polarizations of the two optical fields, and impose restrictions on experimental arrangements. Spatial filtering has been successfully implemented in most cold atom experiments; however, experimental realizations of EIT in a warm atom system require nearly collinear propagation of the signal and control fields to avoid large two-photon Doppler broadening of the EIT resonance. Thus, an appropriate spatial filter must efficiently discriminate two optical fields propagating at very small angle with respect to each other.

In this paper, we present a proof-of-principle demonstration of an optical vortex filter (OVF) that we used to detect a weak probe laser field in the presence of a strong coherent control field under conditions of EIT. This filtering method is largely insensitive to the polarizations and frequencies of two optical fields and thus lacks the complications associated with spectral and polarization filtering mentioned above. It can also be used in conjunction with other filtering methods, if a single filtering method is not sufficient.

An optical vortex, also known as a phase singularity or screw dislocation [14], is a zero of optical field intensity within an otherwise nonzero field. The cross-sectional field amplitude of a beam carrying an optical vortex can be described, in polar coordinates r and θ, as

$$E(r,\theta) \propto \left(\frac{r}{w_0}\right)^m \exp\left[-\left(\frac{r}{w_0}\right)^2\right] \exp[im\theta], \qquad (1)$$

where w_0 is the beam waist, and m is the topological charge of the vortex, which characterizes the number of 2π phase variations within the vortex.

In principle, an optical vortex beam is created by transmitting a Gaussian laser beam through a transparent phase mask having azimuthally varying thickness, $m\lambda_0\theta/(2\pi\Delta n)$, where λ_0 is the specified wavelength and Δn is the refractive index difference between the mask and its surroundings. After the mask, the beam acquires a spatial profile with an azimuthally harmonic phase $\phi = m\theta/(2\pi)$. In the center of the mask, the phase is undefined, and the transmitted beam interferes destructively, creating a region of zero intensity. However,

due to the manufacturing difficulty of creating a smooth spiral mask of this type, a "spiral staircase" mask is typically manufactured. In our experiment, the phase plate was nominally designed to produce a first-order ($m = 1$) optical vortex at $\lambda_0 = 850\,\text{nm}$, but it worked well for 795 nm, as we use below. The mask had eight etched "steps," such that its thickness as a function of the azimuthal angle θ can be described as $d = d_0 - \lambda_0/\Delta n\lfloor 8\theta/(2\pi)\rfloor$, with $d_0 = 0.4\,\text{mm}$, and where $\lfloor\ldots\rfloor$ indicates usage of the floor function. A schematic of such a phase mask is portrayed in the inset of Fig. 1, wherein the gray-scale value corresponds qualitatively to the thickness of each wedge. This phase mask produced the same destructive interference at its center—resulting in a region of zero intensity—but produced unwanted diffraction, owing to the sharp discontinuities at the step boundaries.

The basic idea of an OVF is the following: both overlapping optical fields are focused on the vortex mask such that the unwanted control field is aligned with its center and is converted into an optical vortex beam. The probe field, which propagates at a small angle, does not impinge on the center of the mask, and thus is not affected by the mask. As a result, after the vortex mask, the probe beam propagates within the dark core of the control field beam, and the bright portion of the control field can be blocked with an appropriately sized aperture, leaving only the probe discernible. Similar OVFs have been effectively used to distinguish a dim signal from a stronger background in several applications, such as the detection of extrasolar planets [15–17] and incoherent scattering [18].

In our experiment, we used a prototype OVF to detect the EIT resonance in a Λ system formed by control and probe optical fields tuned to the $5S_{1/2}F = 2 \rightarrow 5P_{1/2}F' = 2$ and $5S_{1/2}F = 1 \rightarrow 5P_{1/2}F' = 2$ transitions of the D_1 line of ^{87}Rb ($\lambda = 795\,\text{nm}$), correspondingly. Both optical fields have the same circular polarization. The attractive feature of such polarization arrangement is that it can be accurately approximated by a simplified three-level Λ system [19], but so far it has been limited to experiments with weak classical probe fields, since it does not allow polarization filtering.

The experimental setup for evaluation of the OVF performance is shown in Fig. 1(b). Both probe and control fields were derived from the same external cavity diode laser (ECDL) to preserve their mutual phase coherence. The two beams were separated on a polarizing beam splitter. The transmitted (more powerful) beam passed through an acousto-optical modulator (AOM), and the first diffraction order with its frequency shifted by –80 MHz was used as a control field in EIT experiment. The reflected beam was phase modulated using an electro-optical modulator (EOM) at frequency 6.7547 GHz, which matches the hyperfine splitting of ^{87}Rb ground state levels (6.8347 GHz) minus 80 MHz. The +1 modulation sideband was then filtered using a temperature tuned Fabry-Perot etalon (FPE) and served as a probe field. The other EOM modulation sideband and the main carrier were suppressed by a factor of approximately 1∶100; moreover, since the modulation frequency differed from the hyperfine splitting, they do not affect probe field propagation through nonlinear mixing. The control and probe beams were then recombined in a nonpolarizing beam splitter cube (NPBS) at a small angle $\alpha = 0.92\,\text{mrad}$ and converted into parallel circular polarizations by a quarter-wave plate ($\lambda/4$) placed before the cell. Both probe and control beams had similar divergence of approximately 0.38 mrad, so it was impractical to separate them even after long propagation.

The powers of the control and probe fields before entering the Rb cell were correspondingly 1.15 mW and 40 μW, and their respective diameters were 1.52 and 0.47 mm. The Rabi frequency corresponding to the control field is $\Omega_C = (2\pi)5.4\,\text{MHz}$, which is calculated as in Ref. [19]. A cylindrical Pyrex cell (length $L = 7.5\,\text{cm}$ and diameter 2.5 cm) containing isotopically enriched ^{87}Rb and 5 Torr of Ne buffer gas was mounted inside three-layer magnetic shielding to reduce the influence of stray magnetic fields. The collisionally broadened optical transition linewidth was $2\gamma = (2\pi)30.3\,\text{MHz}$ [20]. The temperature of the cell was maintained at 50.0 °C, which corresponded to an optical depth of $2d = 47$. Our procedure for calculating the optical depth is described in Ref. [19]. Under these experimental conditions, the linewidth of the EIT resonance is $\Gamma_E = \Omega^2/(\sqrt{d}\gamma) \approx (2\pi)200\,\text{kHz}$ [21]. The Doppler broadening due to the angular separation between control and probe beams is $\Delta_D = (\mathbf{k}_C - \mathbf{k}_p)\cdot\mathbf{v}_{\text{atoms}} \approx \frac{2\pi}{\lambda}u\alpha$ [22], where $u = \sqrt{2k_BT/m_{Rb}}$ is the most probable speed of a Rb atom of mass m_{Rb} at temperature T, and k_B is the Boltzmann constant. For our operating parameters, $u \approx 250\,\text{m/s}$. Thus, for angles $\alpha > \Gamma_E\lambda/(2\pi u) \approx 0.63\,\text{mrad}$, the residual Doppler shift is comparable to or greater than the EIT linewidth. The angle chosen for this experiment ($\alpha = 0.92\,\text{mrad}$) will thus result in minimal Doppler broadening.

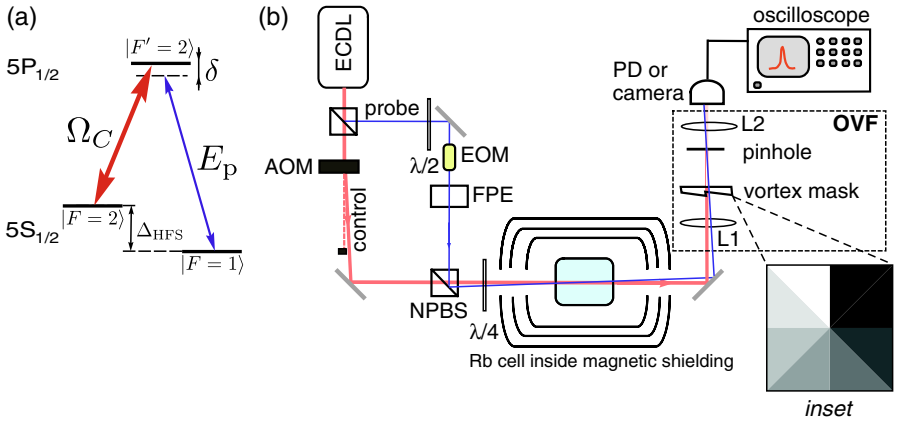

Fig. 1. (Color online) (a) Three-level Λ-type system under conditions of EIT, where Ω_C is a strong control field, E_p is a weak probe field, Δ_{HFS} is a hyperfine splitting between two ground state sublevels, and δ is a two-photon Raman detuning. (b) Schematic of the experimental setup. See text for abbreviations. Inset: schematic of the phase mask described in the text. The gray-scale value corresponds to the thickness of each wedge.

The OVF after the cell consisted of a bichromatic lens L1 (focal length $f_1 = 35\,\text{mm}$), which focused both control and probe beams onto a spiral mask, described above. The position of the mask was carefully adjusted such that the control field was centered at the spiral and transformed into a vortex beam, as shown in Figs. 2(a) and 2(b). Since the probe field propagated at a small angle, it was focused away from the vortex, and, therefore, its transverse intensity distribution was practically unchanged after the mask. A $150\,\mu\text{m}$ pinhole, placed after the mask, was used to block the bright annulus of the control field while passing the probe field. The second lens, L2 ($f_2 = 100\,\text{mm}$), collimated the beams. The transverse intensity distributions of both beams were recorded with a commercial CCD camera, and their total intensities were measured by a photodiode (PD).

An ideal filter will completely extinguish the control field without affecting the probe field. In reality, however, there are several factors limiting the OVF performance. For example, the vortex mask does not have a continuous thickness, but rather consists of eight steps with sharp boundaries that contribute to diffraction; also, any small manufacturing imperfections in the vortex mask center break conditions for perfect destructive interference and thus increase the amount of light in the dark part of the optical vortex beam. Also, good spatial intensity distributions for both control and probe beams is imperative, since it allows the smallest focal spot sizes at the vortex mask, and reduces diffraction losses at the pinhole.

To characterize OVF performance, we measured the power of the control field with and without the vortex mask and pinhole. The filtering factor, defined as the normalized power reduction of the control field, as a function of a distance between the filter mask and the pinhole, is plotted in Fig. 3(a). As expected, the amount of the transmitted control light decreases when the pinhole is placed farther from the mask. Since the focus of the laser beam is at the vortex mask position, the size of the beam and the central dark spot increases and, thus, less light leaks into the central area where the pinhole is placed. At the same time, even though the spatial profile of the probe field is not affected by the vortex mask, it is still attenuated by the pinhole.

By performing numerical calculations of each beams' propagation through the OVF, we found that the size and the position of the pinhole play a crucial role in both control and probe field attenuation. While the pinhole is necessary to obstruct the bright portion of the control field, diffraction of the vortex through the pinhole can cause the brighter outer ring to leak into the dark center and degrade the filtering quality. Furthermore, diffraction of the signal field leads to unwanted attenuation, as energy is lost to higher-order modes and imperfect matching of the pinhole aperture size to the width of the probe beam.

For our experiments, the observation plane (i.e., the position of PD or camera) was approximately $z = 15\,\text{cm}$ from the vortex. Thus, with a pinhole diameter of $a = 150\,\mu\text{m}$, the diffraction criteria $a^2/(\lambda z) \approx 0.10 \ll 1$, so we are in the Fraunhofer or far-field regime. The far-field diffraction pattern through a circular aperture of radius a can be computed as follows [23,24]:

$$U(\rho,\psi) \propto \int_0^{2\pi}\int_0^{a} E(r,\theta) e^{[-ikr\rho/z\cos(\theta-\psi)]} r\mathrm{d}r\mathrm{d}\theta, \qquad (2)$$

where ρ and ψ are the corresponding radial and azimuthal variables in the observation plane, placed at a distance z, and $k = 2\pi/\lambda$ is the wavenumber of light incident on the aperture. Inserting the expression for $E(r,\theta)$ given by Eq. (1) with $m = 1$, we find

$$U(\rho,\psi) \propto \int_0^{2\pi}\int_0^{a} \left(\frac{r}{w_0}\right) e^{-(r/w_0)^2} e^{i\theta} e^{[-ikr\rho/z\cos(\theta-\psi)]} r\mathrm{d}r\mathrm{d}\theta. \qquad (3)$$

The angular integral can be computed analytically [25], leaving the radial integral:

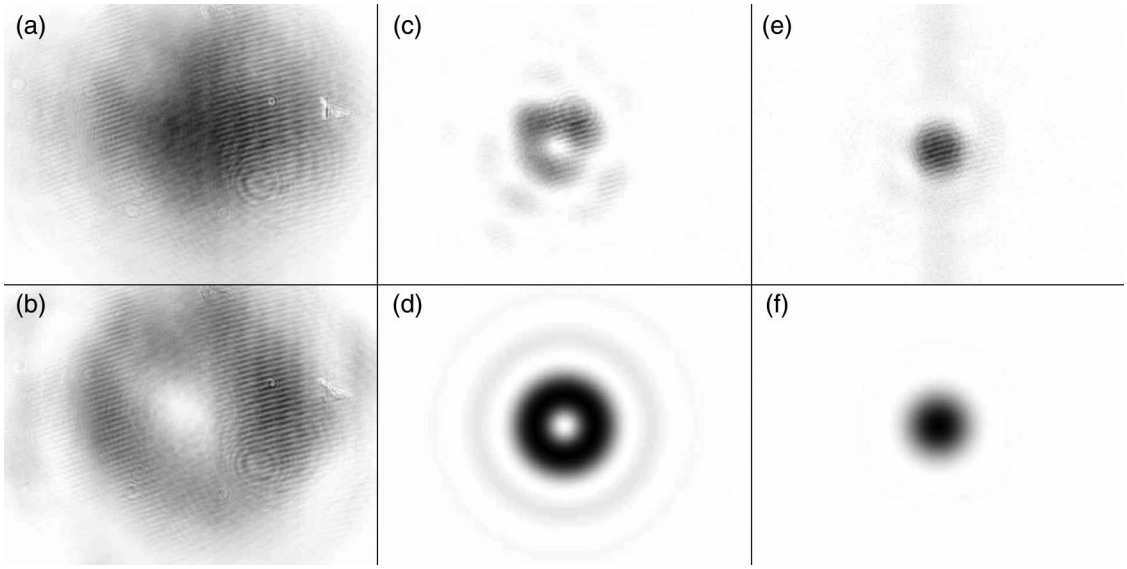

Fig. 2. Left column: measured profiles of the control field (a) before and (b) after the phase mask. Middle column: (c) recorded and (d) calculated diffraction pattern of the optical vortex (the control field after the phase mask) through the pinhole. Right column: (e) recorded and (f) calculated diffraction pattern of the probe field after the phase mask through the pinhole. All images have been inverted in order to exhibit the higher-order diffraction fringes.

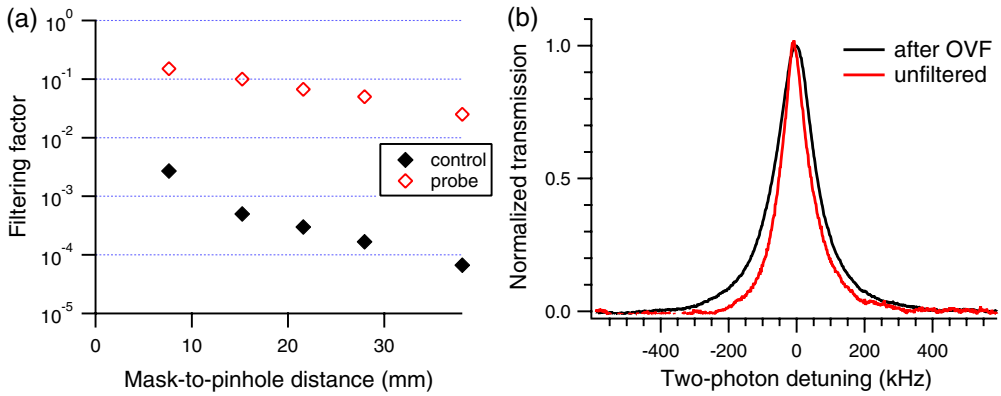

Fig. 3. (Color online) (a) Attenuation of the control and probe fields after OVF. (b) EIT resonance in the probe field, detected after passing through the OVF (black) and without OV filtering (red). For easy line shape comparison, the background is subtracted, and the resonance amplitude is normalized to 1 in both cases.

$$U(\rho,\psi) \propto e^{i(\psi-\pi/2)} \int_0^a \left(\frac{r^2}{w_0}\right) e^{-(r/w_0)^2} J_1(kr\rho/z)\mathrm{d}r, \qquad (4)$$

which can be evaluated via infinite series [24] or numerically. Here, $J_1(x)$ is the first-order Bessel function of the first kind. Similar methods can be used to calculate the diffraction pattern formed by a Gaussian probe pulse through the aperture. Figures 2(d) and 2(f) depict the results from numerically integrating the Fraunhofer diffraction integral for both the control and probe fields. Clearly, they are in a good qualitative agreement with experimental observations shown in Figs. 2(c) and 2(e). We show the inverted images to make the weaker diffraction fringes more discernible. Such calculations can be used to determine the optimal size of the pinhole that simultaneously yields maximum suppression of the control field and maximum transmission of the probe field. Additionally, the calculations confirm that the probe inefficiency is due in large part to a nonoptimal aperture size.

Finally, Fig. 3(b) shows the measured probe EIT resonance recorded with and without optical vortex (OV) filtering (black and red curves, respectively). Although OV filtering does reduce the signal power due to a nonoptimal pinhole size, the method clearly preserves the overall EIT line shape. The small discrepancy between the EIT resonance width is caused by the clipping of the wings of the intensity distribution of the probe field. In this case, with the OVF in place, we effectively detect only the part of the beam with the highest and most uniform control field intensity, which results in a more symmetric power-broadened resonance [black curve in Fig. 3(b)]. Without filtering, the regions with lower intensity (hence smaller power broadening) also contribute, resulting in a overall slightly narrower resonance with a sharper top [26] [red curve in Fig. 3(b)].

In conclusion, we demonstrated the possibility of using an OVF to detect a weak coherent probe field in the presence of a much stronger control field under conditions of EIT. The best demonstrated control field suppression factor is better than 10^{-4}, but this is accompanied by probe suppression, resulting in a filtering efficiency of approximately 10^{-3}. The main limitation of the proposed method—due to the diffraction though the pinhole—can potentially be improved by carefully selecting the pinhole size. Filtering improvement can be made by using a phase mask with higher topological order [15]. The proposed method may be beneficial for a wide range of optical experiments due to its several advantages, such as weak sensitivity to the optical fields' polarization and frequency, as well as only a weak distortion of the probe field wavefront.

ACKNOWLEDGMENTS

The authors thank Kelly A. Kluttz and Carlos Lopez-Mariscal for useful discussions, and G. A. Swartzlander for valuable advice and for loan of one of his phase masks. This research was supported by National Science Foundation (NSF) grant PHY-0758010, and by the College of William and Mary through the summer Research Experience for Undergraduates (REU) program.

REFERENCES

1. M. Fleischhauer, A. Imamoglu, and J. P. Marangos, "Electromagnetically induced transparency: optics in coherent media," Rev. Mod. Phys. **77**, 633–673 (2005).
2. M. D. Lukin, "Colloquium: trapping and manipulating photon states in atomic ensembles," Rev. Mod. Phys. **75**, 457–472 (2003).
3. A. B. Matsko, O. Kocharovskaya, Y. Rostovtsev, G. R. Welch, A. S. Zibrov, and M. O. Scully, "Slow, ultraslow, stored, and frozen light," Adv. At. Mol. Opt. Phys. **46**, 191–242 (2001).
4. R. W. Boyd, "Slow and fast light: fundamentals and applications," J. Mod. Opt. **56**, 1908–1915 (2009).
5. J. Vanier, "Atomic clocks based on coherent population trapping: a review," Appl. Phys. B **81**, 421–442 (2005).
6. V. Shah, S. Knappe, P. D. D. Schwindt, and J. Kitching, "Subpicotesla atomic magnetometry with a microfabricated vapour cell," Nat. Photonics **1**, 649–652 (2007).
7. A. Kuzmich, W. P. Bowen, A. D. Boozer, A. Boca, C. W. Chou, L. M. Duan, and H. J. Kimble, "Generation of nonclassical photon pairs for scalable quantum communication with atomic ensembles," Nature **423**, 731–734 (2003).
8. M. D. Eisaman, L. Childress, A. André, F. Massou, A. S. Zibrov, and M. D. Lukin, "Shaping quantum pulses of light via coherent atomic memory," Phys. Rev. Lett. **93**, 233602 (2004).
9. V. Balic, D. A. Braje, P. Kolchin, G. Y. Yin, and S. E. Harris, "Generation of paired photons with controllable waveforms," Phys. Rev. Lett. **94**, 183601 (2005).
10. A. I. Lvovsky, B. C. Sanders, and W. Tittel, "Optical quantum memory," Nat. Photon. **3**, 706–714 (2009).
11. H. J. Kimble, "The quantum internet," Nature **453**, 1023–1030 (2008).
12. S. Manz, T. Fernholz, J. Schmiedmayer, and J.-W. Pan, "Collisional decoherence during writing and reading quantum states," Phys. Rev. A **75**, 040101(R) (2007).

13. D. Höckel, E. Martin, and O. Benson, "Note: an ultranarrow bandpass filter system for single-photon experiments in quantum optics," Rev. Sci. Instrum. **81**, 026108 (2010).
14. M. Vasnetsov and K. Staliunas, *Optical Vortices* (Nova Science, 1999).
15. G. A. Swartzlander, Jr., "Peering into darkness with a vortex spatial filter," Opt. Lett. **26**, 497–499 (2001).
16. G. Foo, D. M. Palacios, and G. A. Swartzlander, "Optical vortex coronagraph," Opt. Lett. **30**, 3308–3310 (2005).
17. J. Lee, G. Foo, E. G. Johnson, and G. A. Swartzlander, "Experimental verification of an optical vortex coronagraph," Phys. Rev. Lett. **97**, 053901 (2006).
18. D. Palacios, D. Rozas, and G. A. Swartzlander, "Observed scattering into a dark optical vortex core," Phys. Rev. Lett. **88**, 103902 (2002).
19. N. B. Phillips, A. V. Gorshkov, and I. Novikova, "Optimal light storage in atomic vapor," Phys. Rev. A **78**, 023801 (2008).
20. M. D. Rotondaro and G. P. Perram, "Collisional broadening and shift of the rubidium D_1 and D_2 lines $(5^2S_{1/2} \rightarrow 5^2P_{1/2}, 5^2P_{3/2})$ by rare gases, H_2, D_2, N_2, CH_4 and CF_4," J. Quant. Spectrosc. Radiat. Transfer **57**, 497–507 (1997).
21. M. D. Lukin, M. Fleischhauer, A. S. Zibrov, H. G. Robinson, V. L. Velichansky, L. Hollberg, and M. O. Scully, "Spectroscopy in dense coherent media: line narrowing and interference effects," Phys. Rev. Lett. **79**, 2959–2962 (1997).
22. P. R. S. Carvalho, E. E. de Araujo, Luís, and J. W. R. Tabosa, "Angular dependence of an electromagnetically induced transparency resonance in a Doppler-broadened atomic vapor," Phys. Rev. A **70** 063818 (2004).
23. M. Born and E. Wolf, *Principles of Optics* (Pergamon, 1965).
24. G. Lenz, "Far-field diffraction of truncated higher-order Laguerre-Gaussian beams," Opt. Commun. **123**, 423–429 (1996).
25. I. S. Gradshteyn and I. M. Ryzhik, *Table of Integrals, Series, and Products* (Academic, 2000), Section 3.937.
26. A. V. Taichenachev, V. I. Yudin, M. Stahler, J. Kitching, R. Wynands, and L. Hollberg, "On dependence of the shape of nonlinear resonance on a spatial distribution of light beams intensity," in *Technical Digest of International Quantum Electronics Conference* (Optical Society of America, 2002), p. 337.